

International Journal of Modern Physics E
© World Scientific Publishing Company

Mapping out the jet correlation landscape: a perspective from PHENIX experiment

Jiangyong Jia for the PHENIX Collaboration
*Chemistry Department, State University of New York at Stony Brook,
Stony Brook, NY 11794-3400, USA*

*Physics Department, Brookhaven National Laboratory,
Upton, NY 11796, USA
jjia@bnl.gov*

This is a status report on where PHENIX stands in terms of mapping out the landscape of jet correlation in p_T , hadron species, \sqrt{s} . We discuss separately high p_T correlation results and low and intermediate p_T correlation results. The former is sensitive to the quenching of the jet by medium, the later allows detailed study of the medium response to the (di-)jet.

Contents

1	Introduction	2
2	p_T evolution of correlation pattern	3
3	Medium response	5
3.1	Hadron-hadron correlation	5
3.2	Three particle correlation	11
3.3	Identified hadron-hadron correlation	12
3.4	Comments on v_2 background subtraction	14
3.5	The meaning of per-trigger yield	16
4	Jet quenching	18
4.1	hadron-hadron and π^0 -hadron correlation at high p_T	18
4.2	γ -hadron correlation	21
5	Conclusion and outlook	23

2 *Jiangyong Jia*

1. Introduction

One of the primary focus of the RHIC program is to study the properties of the strongly interacting quark-gluon plasma (sQGP) with high transverse momentum (p_T) jet and dijets. The properties of the plasma can be deduced in two ways: on the one hand, the suppression of single jets and di-jets signals at high p_T tells us about the stopping power or the transport properties of the medium. On the other hand, study the the response of the medium to the jets, especially their energy dissipation in the medium, can reveal the collective properties or equilibration process of the medium.

The studies of two particle azimuth correlation at RHIC have revealed detailed information on the jet interaction with the medium, beyond what we learned from the single particle spectra measurements. Experimentally, any deviations of the correlation pattern in heavy-ion collisions from that in baseline p+p collisions are attributed to some sort of medium effects. Such deviations are found to be dependent on the p_T of the trigger hadrons ($p_{T,T}$) and partner hadrons ($p_{T,A}$). Fig.1 show a schematic sketch of the landscape of the two particle correlations in $p_{T,T}$ or $p_{T,A}$. Based on existing experimental results and theoretical calculations, the while p_T range is divided into four regions, each of which is probably sensitive to different physics. At high p_T , STAR¹ shows that the away side jet magnitude is suppressed by factor of 4-5 relative to p+p, but maintaining a relatively unmodified shape. It is consistent with the fragmentation of the primary jets that survives the medium either through tangential emission² or punching-through mechanisms³ or both⁴. At intermediate p_T range(1-4 GeV/c), the away side jet is broadened⁵ or even concave like⁶ in shape but its amplitude is enhanced relative to p+p⁷. The features were believe to be the consequence of the response of the medium to the energy degradation of the high p_T jets. Many theoretical scenarios have been proposed in the last few years to describe the energy dissipation processes, including gluon radiation⁸, Cherenkov radiation^{9,10}, “Mach Shock” mechanism¹¹. But deflected jet pictures such as hydrodynamical wake¹² or multiple scattering of the jet by the medium¹³ were proposed as well. The first two models require additional particle production, whereas the other models require redistribution of the momentum/energy among existing particles.

In between these two p_T regions, experimental data show an suppressed and possibly very flat away side with no visible peak structure¹⁴. This region (we call moderately high p_T region) could have contributions from both jet fragmentation and responses of the medium. The flat but still positive structure could be the combined result of a fragmentation contribution concentrated around $\Delta\phi = \pi$ and a medium contribution centered at 1 radian away from π . The flat structure probably implies the two components have roughly equal yield at this p_T region.

Lastly is the low p_T region. In most jet quenching models^{15,8}, the bremsstrahlung radiation was believed to be largely contained in a narrow angular range (0.5 rad) around the jet axis. These gluons might be the precursor of

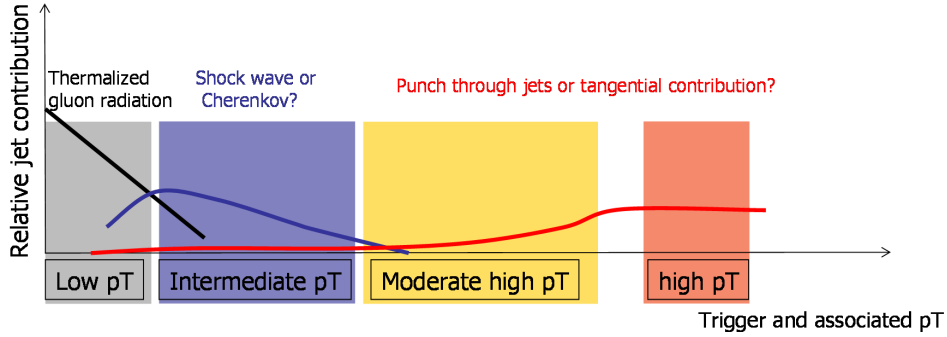


Fig. 1. A sketch of possible contributions to the away side jet yield as function of p_T of triggers and/or partners. The p_T axis is schematically divided into four different regions. It is chosen such that the $p_{T,T} \geq p_{T,A}$ (see Fig.16)).

the collective medium response, but it is also conceivable that some gluons simply thermalized with the medium after additional scattering. In this picture, one would also expect an enhancement in the region around π at low p_T and it should have an exponential thermal shape.

Given that the correlation patterns depend strongly on the p_T of both particles in the pairs, it is crucial to map out the awayside jet properties in a broad p_T range and to identify the transition regions between different correlation patterns. We focus separately on the high p_T region, which is ideal for studying jet quenching and jet tomography, and on intermediate p_T region, which is dominated by the medium response. PHENIX results on hadron-hadron, identified hadron-hadron and three particle correlation are discussed in this context, with an emphasize on new results we have shown in QM2006.

2. p_T evolution of correlation pattern

In correlation analysis, one correlate hadrons in one p_T region (“trigger”) with those in another p_T window (“partner”). The hadron pairs from same jet tend to appear at $\Delta\phi = |\phi_A - \phi_B| \sim 0$ and those from for back-to-back dijet tend to appear at $\Delta\phi \sim \pi$. We are interested in the partner yield distribution per-trigger, $Y_{\text{jet}}(\text{PTY})$, which is defined in a way similar to the previous $d + Au$ and $p + p$ analysis^{16,17}:

$$Y_{\text{jet}} = \frac{\int d\Delta\phi N^{\text{mix}}}{2\pi N_t \epsilon} \left(\frac{N^{\text{fg}}(\Delta\phi)}{N^{\text{mix}}(\Delta\phi)} - \xi (1 + 2v_2^t v_2^a \cos 2\Delta\phi) \right)$$

with the additional $2v_2^t v_2^a \cos 2\Delta\phi$ term to take into account the flow modulation of the background pairs in Au+Au collisions. N_t is the number of trigger, ϵ is the efficiency for associated hadrons in full azimuth and in ± 0.35 pseudo-rapidity. $N^{\text{fg}}(\Delta\phi)$ and $N^{\text{mix}}(\Delta\phi)$ are same-event pair and mixed-event pair distributions,

4 *Jiangyong Jia*

respectively. The superscript t and a stands for the trigger and partner particles. ξ is a normalization factor which is the ratio of the combinatorics pairs in the same event to those in the mixed event. ξ is typically bigger but very close to 1.

Fig.2 shows the PTY for various combination of trigger and partner p_T in central Au+Au collisions, in comparison with p+p. The partner p_T is constrained to be less than trigger p_T . From left to right and top to bottom, the p_T ranges of one or both particles increase, going from $3-4 \times 0.4-1$ GeV/ c (trigger p_T vs partner p_T) to $5-10 \times 5-10$ GeV/ c . The solid lines around the points represent the error due to the elliptic flow uncertainty, which peaks at 0 and π and is the dominating error at $p_T < 3$ GeV/ c . The shaded bands indicate the error due to uncertainty on the background level which is fixed by the Zero Yield At Minimum (ZYAM) method¹⁸. This error depends on the statistical uncertainty at the ZYAM minimum and is the dominating at $p_T > 3$ GeV/ c .

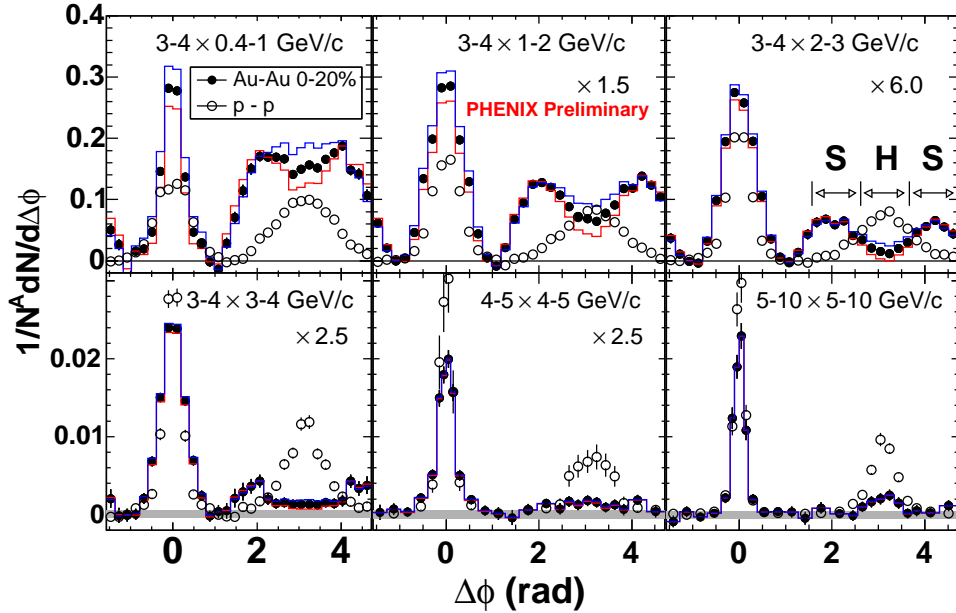


Fig. 2. The yield of associated hadron per-trigger in $\Delta\phi$ for successively increasing $p_{T,T}$ and $p_{T,A}$ in 0-20 % Au+Au collisions. The two lines around the data indicate the errors due to uncertainty of elliptic flow; the shaded bands around 0 indicate the uncertainty from ZYAM method.

The top row shows the jet yield in three successive partner p_T ranges covering 0.4 to 3 GeV/ c with trigger p_T fixed in 3-4 GeV/ c . The away side jet shapes are dramatic different between Au+Au and p+p. The p+p data always peak at π ; The Au+Au data show a concave shape with a dip around π and two side peaks around 1 radian from π . The concaveness grows with increasing partner p_T , however the location of the side peaks is not changing. To characterize the

distorted away side jet shape, we divided the away side into a “Head” region ($\pi/6 < |\Delta\phi - \pi|$) and a “Shoulder” region ($\pi/6 < |\Delta\phi - \pi| < \pi/2$), as illustrated in Fig.1c. They are so named because for normal jet as in p+p, the “Head” region contains bulk of the jet fragmentation, whereas the “Shoulder” contains the tail of the jet fragmentation and the radiative contribution. The “Head” region is sensitive to the level of jet quenching while the “Shoulder” region is suitable for studying the medium response. Clearly, the behavior of the Au+Au data in the two regions are dramatically different from that of p+p. Namely there a suppression in the “Head” region and an enhancement in the “Shoulder” region. The suppression in the “Head” region sets in around 1 GeV/c and grows with larger partner p_T , while the enhancement in the “Shoulder” region persists up to 4 GeV/c.

In the bottom panels of Fig.2, as the p_T of both hadrons are further increased, the awayside “displaced” peaks in Au+Au data seem to be compressed relative to p+p and the Au+Au near side. This reflects the fact that the away side yield drops faster than the near side with increasing partner p_T . In 4-5 GeV/c bin, the Au+Au away side is broader than p+p but is no concave. At the highest p_T bin (5-10 GeV/c), the away side turns into a convex shape, similar in shape to p+p but it’s magnitude is largely suppressed.

Note that medium modification is on the pairs. Thus the shape of the away side should be symmetric with respect to the trigger p_T and partner p_T . Fig.2 suggests that the away side can be categorized in following four regions depends on the $p_{T,T}$ and $p_{T,A}$ based on its shape: 1) a flat region at $p_{T,T}$ or $p_{T,A} < 1$ GeV/c; 2) a concave shape region at $1 \lesssim p_{T,T}, p_{T,A} \lesssim 4$ GeV/c; 3) a convex region $p_{T,T}, p_{T,A} \gtrsim 5$ GeV/c; 4) a transition region (almost flat away side) $p_{T,T}(p_{T,A}) \gtrsim 5$ GeV/c $p_{T,A}(p_{T,T}) \lesssim 3$ GeV/c.

3. Medium response

3.1. Hadron-hadron correlation

PHENIX have tried different methods to quantify the behavior of the away side concave shape at intermediate p_T . The location of the side peaks are characterized by “D”⁶: the distance of the peak to π . “D” is found by triple gauss function fit of the away side:

$$J(\Delta\phi) = G_N(\Delta\phi) + G_A(\Delta\phi - \pi - D) + G_A(\Delta\phi - \pi + D) \quad (1)$$

Fig.3 show D for several collision systems and collisions energies. The position of the peaks was found to be around 1 radian from π independent of the centrality ($N_{\text{part}} > 100$), collision energy and system size. In addition, “D” was found to be relatively insensitive to the change of partner p_T ⁶, which is also confirmed in Fig.2. This suggests that “D” reflects some kind of universal properties of the medium, such as the speed of sound as suggested by the Mach Cone mechanism. It can’t be described by Cherenkov gluon radiation models^{9,10} or most of the deflected

6 *Jiangyong Jia*

jet models such as hydrodynamical wake¹² or Markov random scattering¹³. Such mechanisms would predict narrowing of the peak angle with increasing p_T .

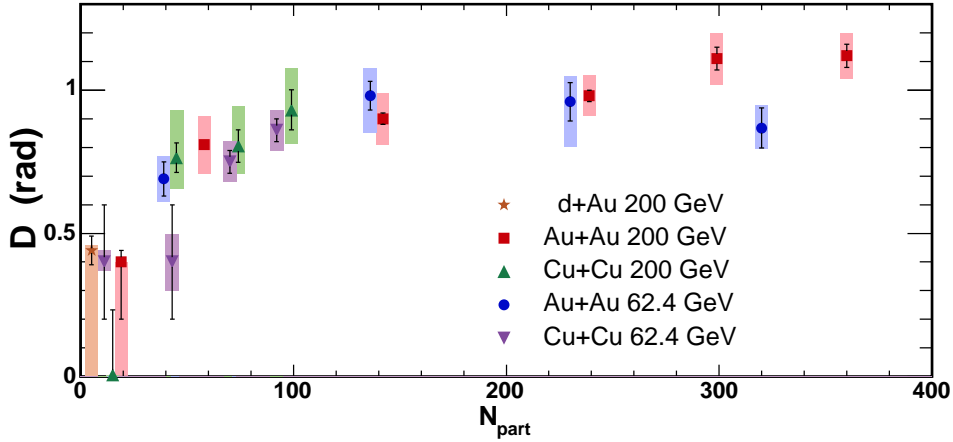


Fig. 3. Collision centrality, energy, and system size dependence of shape parameters “D”.

PHENIX also try to characterize the convexity of the away side jet shape with the ratio of average jet yield in the “Head” region to that in the “Shoulder” region, R_{HS} ,

$$R_{\text{HS}} = \frac{\int_{\text{Head}} d\Delta\phi Y_{\text{jet}}(\Delta\phi)}{\text{Head}} \bigg/ \frac{\int_{\text{Shoulder}} d\Delta\phi Y_{\text{jet}}(\Delta\phi)}{\text{Shoulder}} \quad (2)$$

Each of the distribution in Fig.2 produces one value of R_{HS} that captures essence the the away side jet shape. In general, one expect $R_{\text{HS}} < 1$ for a concave shape, $R_{\text{HS}} \approx 1$ for a flat distribution and $R_{\text{HS}} > 1$ for a convex shape. Thus R_{HS} is an ideal quantity for studying the transition between the “Shoulder” dominated region to “Head” dominated region in p_T . Note R_{HS} is purely a shape variable, thus it is symmetric with respect to $p_{T,T}$ and $p_{T,A}$, i.e. $R_{\text{HS}}(p_{T,T}, p_{T,A}) = R_{\text{HS}}(p_{T,A}, p_{T,T})$.

Fig.4 summarize the $p_{T,T}$ and $p_{T,A}$ dependence of R_{HS} in p+p and central Au+Au collisions. It is presented in fine bins of partner p_T for three trigger p_T regions. The wide red shaded error bars represent the elliptic flow error, which is correlated in p_T ; The narrow green shaded bar represent the ZYAM error, which can vary from point to point. In p+p collisions, R_{HS} is always above one and increases with $p_{T,A}$. This suggests that the away side is always peaked around π in p+p and its width narrows with increasing $p_{T,A}$. The same ratio in 0-5% central Au+Au collisions are drastically different. For trigger p_T in 2-3 GeV/c, R_{HS} decrease from around 1 at $p_{T,A} < 1$ GeV/c to a level of 0.3 ± 0.1 at 3-4 GeV/c. For trigger p_T in 4-5 GeV/c, the decrease of R_{HS} is less significant. The level at low partner p_T is around 1, relatively insensitive to the trigger p_T . This suggests that away side is

flat at low partner p_T independent of the trigger p_T .

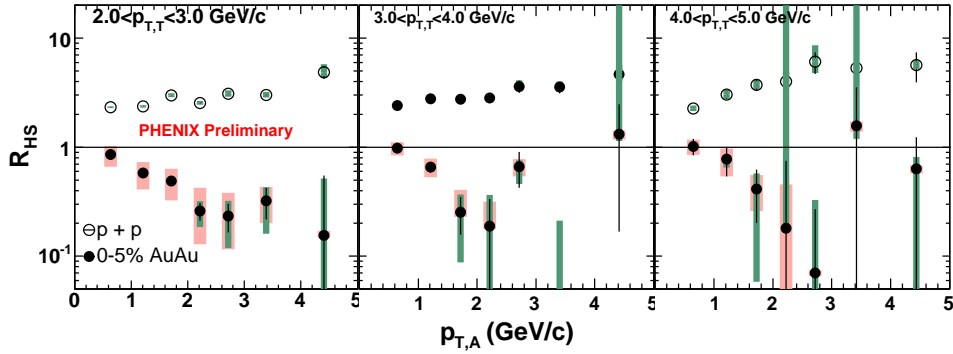


Fig. 4. R_{HS} (The ratio of the average yield in head and shoulder region) as function of $p_{T,A}$ in three $p_{T,T}$ ranges for 200 GeV 0-5% central Au+Au and p+p. Concave $R_{HS} < 1$, flat $R_{HS} \approx 1$, convex $R_{HS} > 1$.

Fig.2 suggests that not only the away side jet shape but also the jet multiplicities are modified in central Au+Au collisions relative to that in p+p. The modifications depend on trigger p_T , partner p_T and $\Delta\phi$ and can be quantified by I_{AA} , the ratio of PTY in Au+Au to that in p+p within a certain $\Delta\phi$ window W:

$$I_{AA}^W = \int_{\Delta\phi \in W} d\Delta\phi Y_{jet}^{Au+Au} / \int_{\Delta\phi \in W} d\Delta\phi Y_{jet}^{p+p} \quad (3)$$

The top panels Fig.5 show the I_{AA} as function of partner p_T at away side ($|\Delta\phi - \pi| < \pi/2$) for three trigger p_T bins. I_{AA} is greater than 1 at low partner p_T but drops towards high partner p_T . This implies that central Au+Au data have a significant enhancement at low partner p_T and a strong suppression at high partner p_T . For higher trigger p_T , the enhancement at low partner p_T is smaller and the suppression at high partner p_T is stronger. The point where I_{AA} cross 1 shifts to lower partner p_T , indicating a stronger decrease of I_{AA} in partner p_T for higher trigger p_T . The observed $p_{T,T}$ and $p_{T,A}$ dependence is a consequence of the competition between the enhancement in the ‘‘Shoulder’’ region and the suppression in the ‘‘Head’’ region shown in Fig.2. At low $p_{T,A}$, the away side is (thus I_{AA}) is dominated by the ‘‘Shoulder’’ region; at sufficiently high $p_{T,A}$, the away side is dominated by the ‘‘Head’’ region. The point where $I_{AA} = 1$ would depend on both trigger and partner p_T . For 4-5 GeV/c trigger, the suppression level seems to saturates around 0.3 at $p_{T,A} > 3$, close to the R_{AA} value for 4-5 GeV/c inclusive hadrons.

The bottom panels of Fig.2 show the I_{AA} as function of partner p_T at away side ($|\Delta\phi| < \pi/3$) for the same three trigger p_T bins. We see similar enhancement at low partner p_T , and the enhancement diminishes towards high partner p_T . As one increase the trigger p_T , the dependence on partner p_T weakens, and the I_{AA} distributions become flatter in partner p_T . The near side enhancement has been

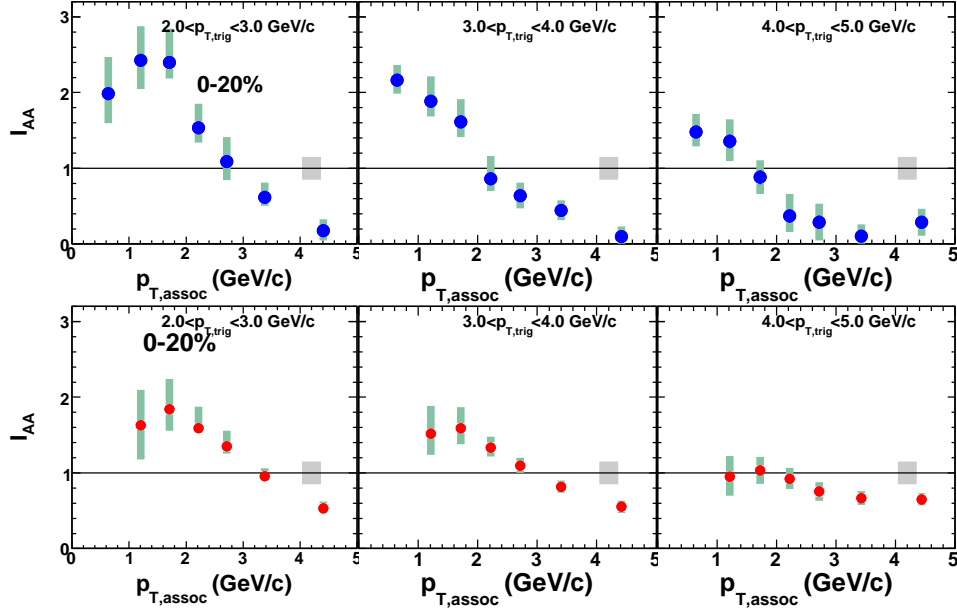
8 *Jiangyong Jia*


Fig. 5. I_{AA} for three different trigger bins in the away side (top panels) and the near side (bottom panels) in 0-20% central Au+Au collisions at 200 GeV.

observed by STAR⁷ and PHENIX^{19,5}, this enhancement was attributed by STAR to the a ridge contribution which extends out in $\Delta\eta$ up to ± 2 . The ridge contribution seen by STAR in $|\Delta\eta| \leq 1.7$ is about factor of three compare to the pure jet contribution, and was argued to be reason for the near side enhancement. The enhancement seen in PHENIX is smaller than observed in STAR, because of the ridge yield in PHENIX's limited η acceptance is smaller. The decrease of the enhancement with increasing trigger p_T suggests that the ridge component is softer than the jet component. The p_T range where the ridge yield is important seems to be in $p_{T,T}, p_{T,A} < 4$ GeV/c, very similar to the range for the enhancement at the away side. PHENIX have also observed a broadening of the near side jet width in central Au+Au collisions²⁰ at intermediate p_T , the broadening was found to disappear at high trigger p_T ²¹ (also see Fig.16). These observations are summarized in Fig.6. The width results are also suggestive of a ridge contribution that is important at intermediate p_T but disappears at large p_T . Due to its limited η acceptance, PHENIX so far haven't be able to observe the ridge signature directly. However, the detailed study of near side jet shape and yield in broad p_T range can provides indirect but still valuable constrains on the properties of the ridge.

PHENIX have carried out the intermediate p_T correlation analysis at both $\sqrt{s_{NN}} = 200$ and 62.4 GeV⁶. CERES also carried out similar analysis at $\sqrt{s_{NN}} = 17.2$ GeV selection²². The results from the three collision energies for

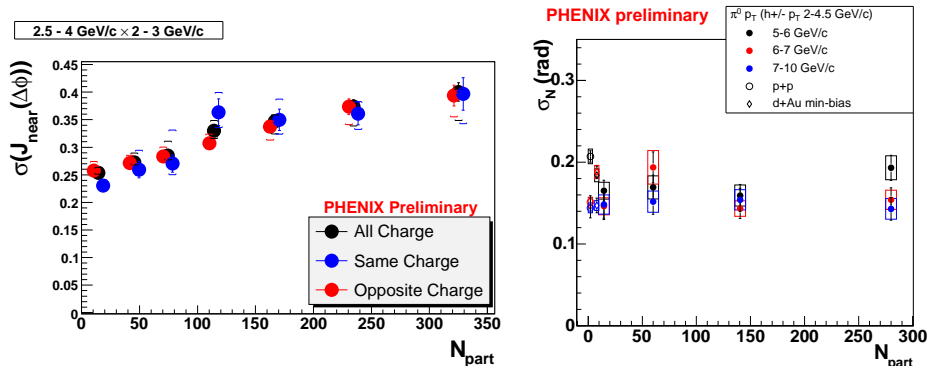


Fig. 6. Centrality dependence of the near side gauss width in 200 GeV Au+Au collisions at intermediate p_T of $2.5 - 4 \times 2 - 3$ GeV/c (Left) and at various high p_T bins above 5 GeV/c (Right).

$1 < p_{T,A} < 2.5 < p_{T,T} < 4$ GeV/c are summarized in the Fig.7. The middle panel ⁶ shows the “jet fraction”, so the scale can’t be compared directly with the other two panels which show the per-trigger yield. But the jet shape can be directly compared among the three distributions. Fig.7 indicate a clear modification of away side jet at all energies. They all have displaced peaks around 1 radian from π , the concaveness of the away side distributions seems to decrease for lower \sqrt{s} . Since the trigger selection are similar, we expect the away side jet energy would be mostly determined by the trigger p_T , modulo a weak \sqrt{s} dependence of the trigger bias (reflected by $\langle z \rangle$) due to the \sqrt{s} dependence of the parton spectra shape. CERES Time Projection Chamber η range is 2.1-2.7 in lab frame, which corresponds to 0.1-0.7 in CM frame. Thus its rapidity range is 0.6 and is close to PHENIX range of 0.7. Thus the jet yield at 17.3 GeV can be compared directly with that at 200 GeV after multiplied by $0.7/0.6 = 1.17$ to correct for the difference in η acceptance. The maximum and minimum value is 0.17 and 0.07 for 0-5% central Au+Au collisions at 200 GeV (Fig.7a) and 0.08 and 0.07 for 0-5% Pb+Pb collisions at 17.3 GeV after the acceptance correlation (Fig.7c). Thus the amplitude of the displaced peak in CERES is about factor 2 lower than PHENIX value, whereas the level at the “Head” region in CERES is surprisingly close to PHENIX value. This probably suggests that the yield in the “Head” region is dominated by fragments from jet. The jet multiplicity are somewhat higher at RHIC due to smaller $\langle z \rangle$, but jet quenching is stronger at RHIC than that in SPS. The yield at “Shoulder” region is significantly smaller at SPS than at RHIC, possibly suggesting a weaker medium effect. Clearly detailed study of the \sqrt{s} dependence of the “Head” and “Shoulder” yield can provide crucial constrains on interplay between jet quenching and medium response.

PHENIX also obtained some interesting but puzzling results for correlations between very low p_T hadrons ($0.2 < p_T < 0.4$ GeV/c) ²³. Fig.8 shows azimuthal

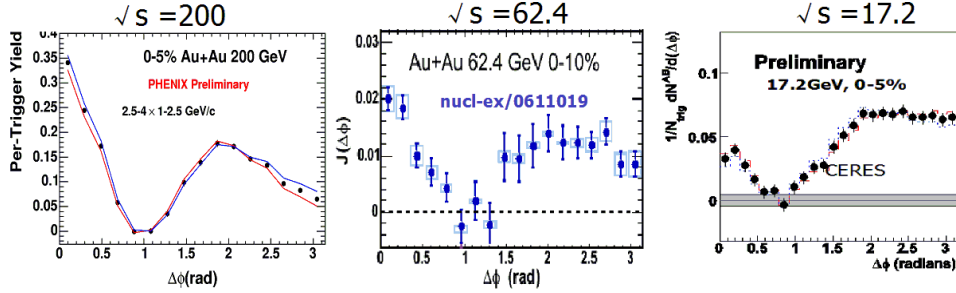
10 *Jiangyong Jia*


Fig. 7. a) Per-trigger yield in central Au+Au collisions at $\sqrt{s_{\text{NN}}} = 200$ GeV from PHENIX. b) The extract jet function at $\sqrt{s_{\text{NN}}} = 62.4$ GeV from PHENIX. c) Per-trigger yield at $\sqrt{s_{\text{NN}}} = 17.2$ GeV from CERES.

correlation in 0-5% Au+Au collisions for like-sign pairs (left) and unlike-sign pairs (right). The like-sign correlation shows a near side peak consistent with HBT correlation, whereas unlike-sign correlation does not. What is surprising is the observation of a displaced peak at a location that is consistent with what has been observed for high p_T correlation. Whether it has the same physics origin is not clear. If this is due to correlation between soft particle in the jets or mini-jets, why the unlike-sign correlation does not show any enhancement at the near side as well (the ridge argument)? It is also worth pointing out that the displaced peak mostly concentrated in a very narrow window of $|\Delta\eta| < 0.1$ and that the peak only shows up in large $N_{\text{part}} \gtrsim 100$ and is insensitive to the collision energy. It is observed at 0-5% Au+Au at 62.4 GeV but not in central Cu+Cu collisions at 200 or 62.4 GeV. Further characterization of the shape and yield of this away side peak is underway to clarify the picture.

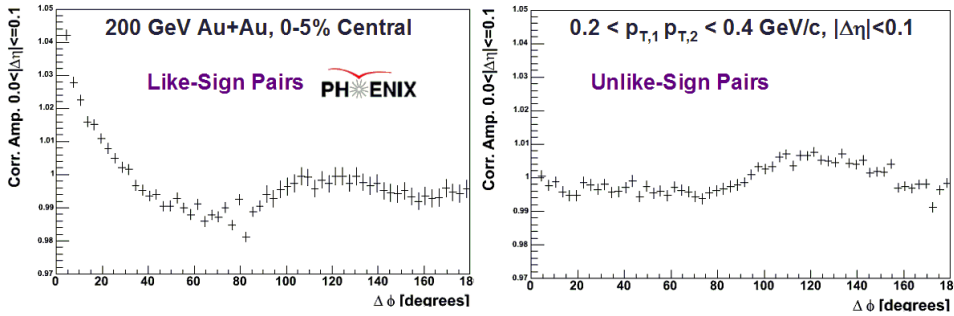


Fig. 8. Low p_T like-sign (left) and unlike-sign correlation function for 0-5% central 200 GeV Au+Au collisions.

3.2. Three particle correlation

Three-particle correlation can provide direct topological features on the interaction of the jets with the medium, thus potentially allows clear distinction of various modification patterns such as Mach-cones and Deflected jets which can't be directly differentiated with two particle correlation method. There are four independent angular variables among the three particles, $\Delta\phi_{12} = \phi_1 - \phi_2$, $\Delta\phi_{13} = \phi_1 - \phi_3$, $\Delta\eta_{12}$ and $\Delta\eta_{13}$. If one is mainly interested in the azimuthal correlation, as is done in STAR²⁴ and in earlier PHENIX measurements²⁵, then there are only two independent variable $\Delta\phi_{12}$ and $\Delta\phi_{13}$. Recently PHENIX has chosen to characterize three particle correlations through the use a local polar coordinate system where the trigger direction is the z axis (see insert of Fig.9)²⁶. In this scheme, the four independent variables are $\theta_1^*, \theta_2^*, \phi_1^*$ and ϕ_2^* . Note that the coordinate system is defined for each trigger so it changes trigger by trigger relative to the global frame. In the data analysis, PHENIX chose $\Delta\theta^* = \theta_1^* - \theta_2^*$ and $\Delta\phi^* = \phi_1^* - \phi_2^*$ as the two independent variables. These two variables combine the information of all four angles, thus provide a very different way of presenting the jet signal.

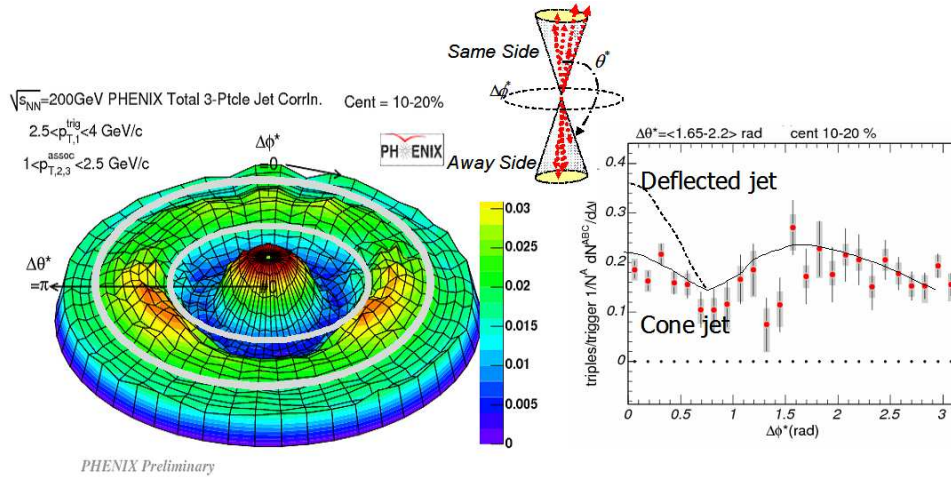


Fig. 9. (Left) Full $\Delta\phi^*$, $\Delta\theta^*$ correlation surface in 10-20% Au+Au collisions. (Middle insert) Schematic illustration of coordinate system. (Right) the 1-D projection of along $\Delta\phi^*$ for $1.65 < \Delta\theta^* < 2.2 \text{ rad}$.

Left panel of Fig.9 shows the resulting three-particle correlation function in $\Delta\theta^*$ and $\Delta\phi^*$. The soft-soft and soft-hard flow backgrounds have been subtracted, but it still includes the 2+1 (two particles from di-jet and one from background) flow background. It is important to note that this correlation function as generated also contains the effect of the PHENIX acceptance. One can see three peaks in the ring region ($1.65 < \Delta\theta^* < 2.2 \text{ rad}$) between the two gray circles, located at $\Delta\phi^* \approx 0$ and

$\Delta\phi^* \approx \pm\pi/2$. These peaks were not observed for simulation where only normal di-jet is included, thus are signatures for the medium effects. After removing the 2+1 flow contributions, right panel of Fig.9 shows the projection along the ring on the $\Delta\phi^*$ axis, together with expectation of simplistic cone jet and deflected jet scenarios given by Monte-Carlo simulations. In both scenarios, one expected a narrow peak around $\Delta\phi^* \approx 0$ and a broad peak around $\Delta\phi^* \approx \pi/2$. The difference is that the deflected jet scenario predicts a bigger jet amplitude at $\Delta\phi^* \approx 0$ than that for the cone jet. From right panel of Fig.9, it appears that the PHENIX measurements are most consistent with the excitation of a Mach cone in the medium and not consistent with a deflected jet hypothesis.

3.3. Identified hadron-hadron correlation

Previous results indicate that the jet properties at the nearside, away-side “Head” and away-side “Shoulder” regions are quite different. The near side is consist of a ridge component along $\Delta\eta$ and a jet fragmentation contribution. The away-side “Shoulder” region is dominated by collective medium response and the “Head” region seems to be consist of jet fragmentation plus possible feedback from the radiated gluons. Given the complexity of the problem and many theoretical possibilities, one need additional handles to test this picture. Correlation with identified particles can reveal the composition or the chemistry of the jet yield in the three regions, thus provide valuable constraints on the underlying physics.

Fig.10 shows the partner meson and baryon yield in 1-1.3 GeV/c (top panels) and 1.6-2.0 GeV/c (bottom panels) for unidentified trigger in 2.5-4 GeV/c. Results for 0-20% and 20-40% Au+Au collisions are shown in the left panels and right panels, respectively. The partner baryon yields are scaled to approximately match the partner meson yields. Clearly, the away side shows a concave shape for both partner mesons and baryons. This is not surprising for partner meson since it dominates the charged hadrons. But it is interesting to see that partner baryons also have a similar but less concave shape (higher in the head region and lower in the shoulder region in the figure).

Fig.11 shows the ratios of the parter baryon/meson yield as function of partner p_T for several centrality bins at the near side (left panel) and away side (right panel). The ratios are compared with that for the inclusive spectra and e^+e^- collisions. The ratio for the near and away side jet grow steadily with increasing partner p_T in all centralities, similar to inclusive hadrons and normal jet fragmentation measured in e^+e^- collisions. But the increase is a little bit stronger in central Au+Au collisions as well as for the away side. The $p/(\pi+k)$ ratio is about 0.1 for pure jet fragmentation and ~ 0.4 for inclusive spectra in central Au+Au collisions. The $p/(\pi+k)$ ratio for the away side jet is somewhere in between. If the Mach-cone scenario is true, it is conceivable that the jet excites the medium at the away side, which then fragments in the usual recombination prescription. This would naturally lead to the centrality dependent baryon/meson ratio in the away side.

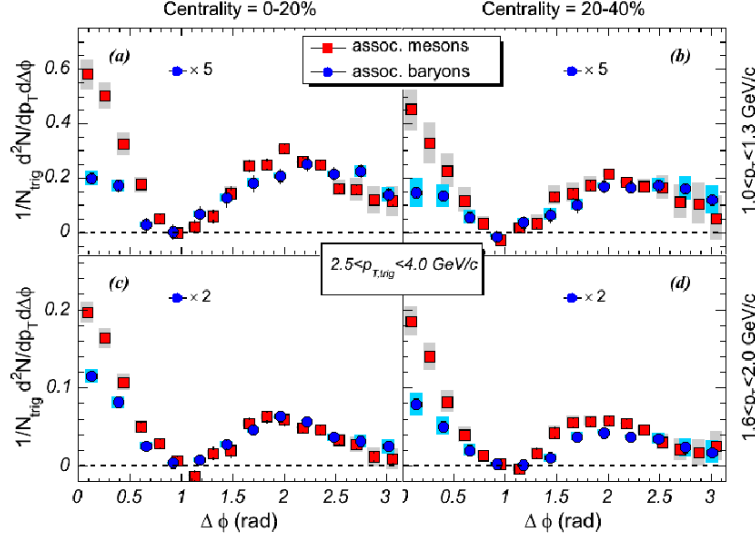


Fig. 10. The associated meson and baryon $\Delta\phi$ distribution for unidentified charged hadron triggers.

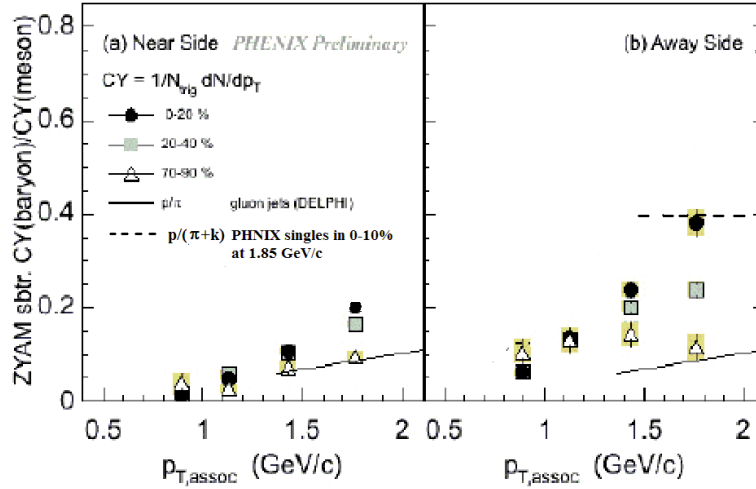


Fig. 11. Ratio of partner baryon to meson at the near side (left panel) and away side (right panel). It is plotted as function of partner p_T for 0-20%, 20-40% and 70-90% centrality bin. Trigger particles are charged hadrons with $2.5 < p_T < 4.0$ GeV/c.

Fig.12 shows the near side yield where the trigger is identified in PHENIX ²⁷(left) compared with results from STAR (right) ²⁸. PHENIX Results show a steady increase with centrality, except a quick drop of the yield for trigger baryon at $N_{\text{part}} > 250$. The increase trend is qualitatively consistent with results

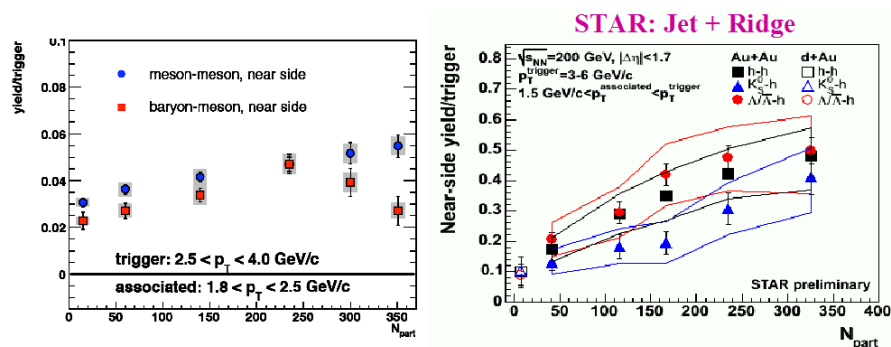
14 *Jiangyong Jia*


Fig. 12. (left) the near PTY in $|\Delta\phi| < 0.94\text{rad}$ for baryon-meson (squares) and meson-meson (circles) correlations as a function of N_{part} . (right) Similar results from STAR.

obtained from hadron-hadron correlation (see Fig.5), which was argued to be due to the ridge in $\Delta\eta$. Similar trend is also observed by STAR in the right panels, except that in their case, the yield for trigger baryon is significantly larger than for trigger mesons and yield for trigger baryon does not drop in central collisions. However we should note that the trigger p_T in STAR is different from PHENIX and they also include more ridge contribution due to a much larger $\Delta\eta$ coverage. In any case, a good theoretical model should be able to simultaneously explain single particle yields, elliptic flow and as well as these PID correlation results. Quark recombination (thermal-thermal and thermal-shower) was quite successful in describing the spectra and elliptic flow, but so far was not very successful in describing the jet correlation yield, especially the centrality dependence²⁷.

3.4. Comments on v_2 background subtraction

One of the important systematic errors in the jet correlation comes from elliptic flow background subtraction (see Eq.1). In the past years, many different methods have been developed to measure the v_2 : Reaction-Plane (RP) Method ($v_2\{RP\}$), 2 particle cumulant method ($v_2\{2\}$), 4 particle cumulant method ($v_2\{4\}$), and SMD-ZDC method (Reaction-plane for direct flow v_1). These measurements have quite different sensitivities on the non-flow effects and eccentricity fluctuation^{29,30,31,32}. The obvious question to ask is what v_2 one should use in the jet correlation analysis?

The two particle correlation method and two particle cumulant method are closely related. Naturally, all non-flow effects and event by event fluctuations that affects the cumulant v_2 would also contribute to the two particle azimuthal correlation. Thus it seems that $v_2\{2\}$ should be used in the background subtraction except that one would like to remove the jet bias to $v_2\{2\}$ since it is the signal. PHENIX use the $v_2\{RP\}$ in all correlation analysis. The $v_2\{RP\}$ is determined by

the BBC which sits in the forward region ($3 < |\eta| < 4$). The RP method measures separately the average v_2 for the triggers ($\langle v_2^t \rangle$) and partners ($\langle v_2^g \rangle$). Due to eccentricity fluctuation, the v_2 of the triggers and partners fluctuate in the same direction event by event. This intrinsic fluctuation would lead to $\langle v_2^t v_2^g \rangle \neq \langle v_2^t \rangle \langle v_2^g \rangle$. Both PHOBOS³³ and STAR³⁴ found a substantial eccentricity fluctuation, around 40%. From it, the additional correction factor can be roughly estimated to be (assuming a gauss shape for the fluctuation):

$$\sqrt{\langle v_2^2 \rangle} \approx \langle v_2 \rangle \left(\sqrt{1 + \left(\frac{\delta v_2}{\langle v_2 \rangle} \right)^2} \right) \approx 1.08 \langle v_2 \rangle \quad (4)$$

So this suggest that the $v_2\{\text{RP}\}$ should be increased by 8% in order to account for the correlated fluctuation between triggers and partners. However, PHENIX have measured both the $v_2\{2\}$ $v_2\{\text{RP}\}$ ³⁵. The agreements between the two methods are better than 8%. Note that Eq.4 is very sensitive to the δv_2 used in the calculation and as well as the gauss smearing assumption. The correction factor would be only 4.5% for a 30% input v_2 fluctuation. So probably the estimation of Eq.4 is too simplistic.

In many jet correlation analyses in STAR, the used v_2 is an average between TPC $v_2\{\text{RP}\}$ and $v_2\{4\}$. Since the $v_2\{4\}$ reduces non-flow as well as fluctuation effects, it is smaller than $v_2\{2\}$. This probably explains why their away side jet shape at intermediate p_T is less concave comparing to PHENIX.

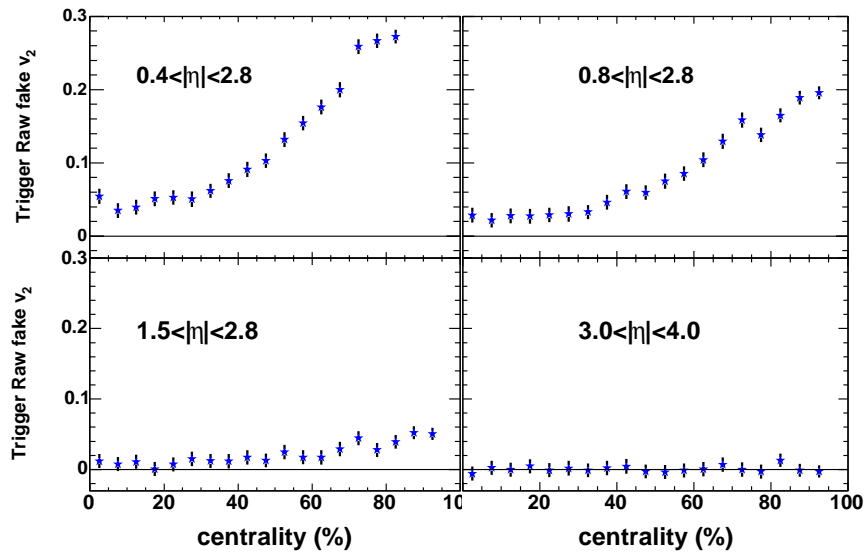


Fig. 13. The fake v_2 of the leading particle from jet as function of centrality using the EP determined in four η windows. The embedded jet is at mid-rapidity ($|\eta| < 0.35$).

One of the advantages of the PHENIX RP v_2 measurement comes from the large pseudo-rapidity gap between BBC and the central arm. This gap greatly reduce the effects of the jet bias on the RP v_2 . PHENIX have perform detailed Monte Carlo simulation to estimate the bias effect. Fig.13 shows the centrality dependence of jet induced fake v_2 for various pseudo-rapidity window used to determine the RP. The fake v_2 decreases as the η window used to determine the RP angle is further away from mid-rapidity. For the η window in BBC acceptance ($3 < |\eta| < 4$), the fake v_2 is almost negligible. Further details can be found in ³⁶.

PHENIX have measured the jet yield as function of angle with respect to the reaction plane at intermediate p_T ²⁰. Due to the smearing effect due to relatively poor RP resolution of BBC and possibly a small jet signal, we see little jet like difference of the per-trigger yield in the in-plane direction relative to the out-plane direction (see Fig.6 of ²⁰ and discussions.). We can use this special property to constrain the v_2 simultaneously using CFs measured at different angular direction. Fig.14a shows the CFs in 0-5% central Au+Au collisions for 6 angular bins in 15° steps. Fig.14b shows the jet yield after subtracting the flow terms which can be calculated according to simple equation ²⁰. Although the CFs change dramatically from in plane to out of plane, the calculated flow term tracks the true flow background nicely. Given the small eccentricity in 0-5%, we can safely assume that the jet yield, jet yield should not depend on the trigger direction. Thus the relatively good agreements between 6 measurements is an independent confirmation of the $v_2\{\text{RP}\}$ used in the correlation measurement. The small remaining difference between the jet functions in Fig.14b can be used to further constrain the v_2 .

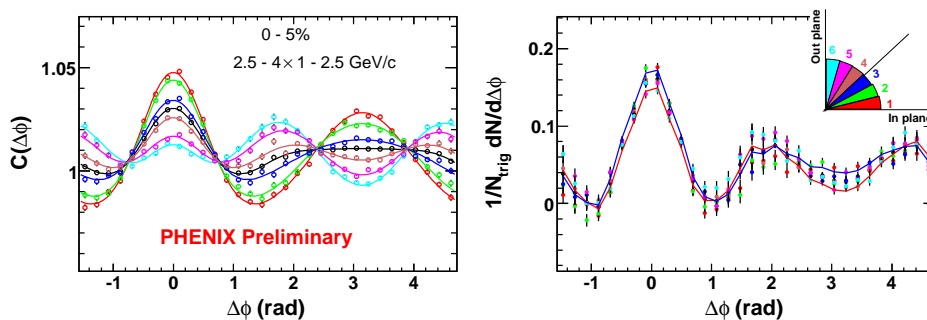


Fig. 14. a) Correlation function for various 6 trigger direction bin and the trigger integrated bin (the center black curve) in 0-5% Au+Au at 200 GeV. b) The background subtracted per-trigger yields, the insert figure shows the 6 trigger bins.

3.5. The meaning of per-trigger yield

In two particle correlation analysis, typically one correlate particles in a high p_T window (type *a*) with those in a low p_T window (type *b*). The distinction between

triggers and partners are arbitrary since medium modifications are on the jet pairs. There is a simple relation between the PTY using the high p_T particles as triggers and that using low p_T particles as triggers:

$$R_{AA}^a I_{AA}^a = R_{AA}^b I_{AA}^b = \frac{\text{JetPairs}_{AA}}{N_{\text{coll}} \times \text{JetPairs}_{pp}} \equiv J_{AA}(p_T^a, p_T^b) \quad (5)$$

where JetPairs_{AA} and JetPairs_{pp} represent the average number of jet pairs in one A+A collision and one p+p collision, respectively. The R_{AA}^a represents R_{AA} for type a particles and I_{AA}^a represents PTY using type a particles as triggers. In naive jet quenching picture, the observed triggers are biased close to the surface, the corresponding away side companions have a larger medium to traverse. One expects $I_{AA} < R_{AA}$ or $J_{AA} < R_{AA} I_{AA}$. In direct photon-jet correlation, since direct photons are not modified by the medium, the away side jet would behave exactly as the single jet suppression: $I_{AA} = R_{AA}$.

In correlation analysis, we are interested in studying the modification of the away side jet tagged by the triggering jet, i.e the **per-jet yield**. In reality we study the modification on the **per-trigger yield**, represented by I_{AA} . The physics interpretation of this quantity are complicated by the modifications on the triggers. In general there can be two types of modifications of the triggers:

- (1) Additional triggers not coming from jet: such as thermal-thermal recombination, boost of soft particles due to flow. They tend to dilution the PTY.
- (2) Pure medium modifications of the triggers: jet quenching, enhancement due to energy dissipation such as radiative gluons/Mach-cone/Cherokov. They either does not affect or increase the PTY.

(2) represents the effects we hope to study, which are complicated by (1). Both can change I_{AA} , but relation Eq.5 always holds. Fig.15 illustrates th idea by showing the PTYs from Au+Au and p+p, where the two hadrons are selected from non-overlapping p_T ranges. In the left panel, 2-3 GeV/c hadrons and 3-4 GeV/c hadrons are used as triggers (a) and partners (b), respectively. In the right panel, the role of triggers and partners are swapped. Clearly, the vertical scale of the left panel is less than that in the right panel, simply because there are many more hadrons in 2-3 GeV/c than 3-4 GeV/c. In the left panel, the nearside Au+Au data points are close to those for p+p; whereas in the right panel, the nearside Au+Au data are higher. This is the case because R_{AA} is smaller in 3-4 GeV/c than in 2-3 GeV/c. More suppression means less number of triggers for fixed number of pairs, thus the PTY increase relative to the p+p value.

Either (1) or (2) can explain this example. We can argue that most of type-a particles come from recombination without jet correlation, thus I_{AA} for type-a is smaller than that for type-b. We can also argue that type-a particles come from jet but are less suppressed than type-b, thus I_{AA} for type-b is larger than that for type-a. v_2 and spectra measurements suggest that a large fraction (more than 50%) of the particles in 2-4 GeV/c come from recombination. However the measured

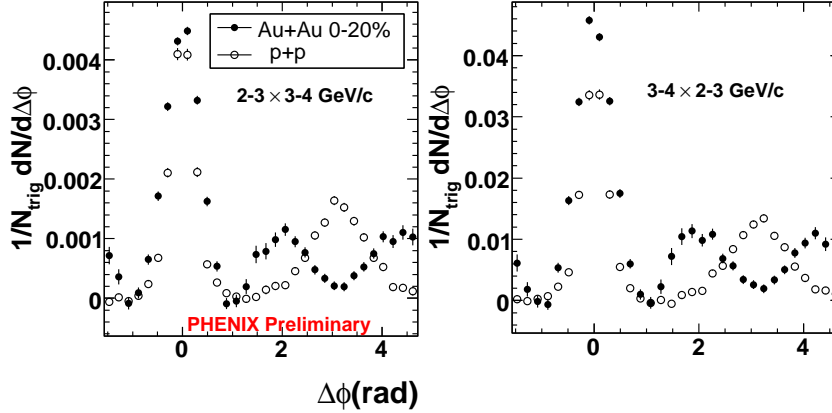


Fig. 15. The per-trigger yield for 2-3 and 3-4 GeV/ c correlation, a) using 2-3 GeV/ c particles as trigger, b) using 3-4 GeV/ c particles as trigger.

per-trigger yield is significantly enhanced at $p_T < 4$ GeV/ c as shown by Fig.5. This suggests that either triggers are dominated by the shower-thermal recombination, hence maintaining the jet correlation, or the enhancement of the jet multiplicity is much bigger than the dilution to the triggers. PID correlation measurement can help to clarify this issue. Fig.12²⁷ indeed shows some differences between baryon and meson triggers on the near side and possibly also on the away side. This trend is not consistent with the dilution from pure thermal-thermal recombination model predictions²⁷. Further high statistics detailed measurement of the PID correlation in intermediate p_T can help clarify the origin of the enhancement.

4. Jet quenching

4.1. hadron-hadron and π^0 -hadron correlation at high p_T

At high p_T , the situation is a lot more cleaner. The dilution to jet yield due to recombination or flow (if there is any) become negligible. Since each jet fragments into one high p_T trigger, the per-trigger-yield at the away side is the same as the per-jet yield. Fig.16 show the centrality dependence of the jet yield for 5-10 GeV/ c trigger and 3-10 GeV/ c partner in 200 GeV Au+Au collisions. The shape and yield at the near side show very little centrality dependence. The away side jet is clearly peaked at π , but the magnitude is significantly suppressed in central Au+Au collisions comparing to that in peripheral collisions, consistent with strong quenching or absorption of the away side jet.

PHENIX also carried out detailed study of the jet correlation analysis in Cu+Cu collisions at 200 GeV. The jet correlation measurements in Cu+Cu offer several unique advantages. In terms of N_{part} , Cu+Cu collisions cover from peripheral to 30-40% central Au+Au collisions. N_{part} can be determined with better precision than in Au+Au, thus allows a more detailed mapping of the centrality dependence

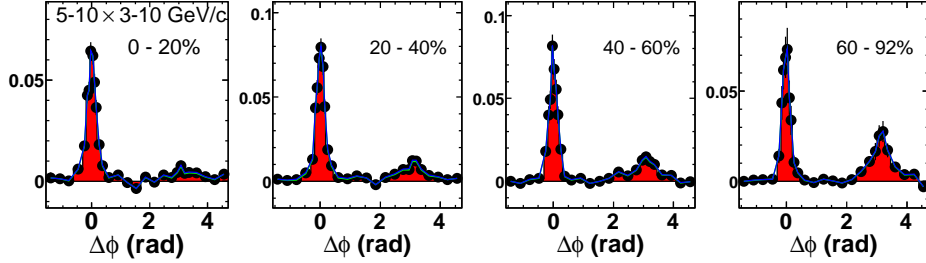


Fig. 16. The hadron - hadron PTY as function of centrality at high p_T in 200 GeV Au+Au collisions.

of the onset of the jet quenching. Secondly, systematic error from v_2 on the jet yield is much smaller in Cu+Cu due to a smaller combinatoric background.

The measurement was carried with 5-10 GeV/c π^0 as triggers and charged hadrons in several ranges in 0.4-10 GeV/c as partners. Fig.17 show the correlation function in 0-20% Cu+Cu compared with that in p+p. A clear away side excess can be seen in all partner p_T ranges. No concave shape is expected even after the v_2 background subtraction. At partner $p_T > 2$ GeV/c, the away side can be well fitted with a gauss function. Fig.18 shows the near side and away side jet width as function of partner p_T for p+p, 0-20% and 20-40% Cu+Cu collisions. No apparent differences can be seen between Cu+Cu and p+p, suggesting partners come mostly from jet fragmentation in the p_T range under consideration (all p_T on the near side and $p_T > 2$ GeV/c on the away side).

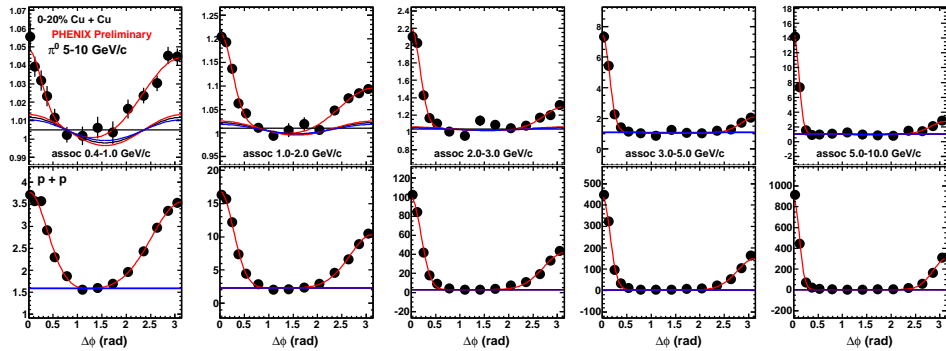


Fig. 17. The correlation function in Au+Au (upper panels) and p+p (bottom panels).

Comparing the top and the bottom panels of Fig.17, one notices that there is a larger asymmetry between the near and away side in Cu+Cu than in p+p. To quantify the medium modifications, we extract the PTY for Cu+Cu and p+p and construct the I_{AA} as function of x_E ($x_E = p_{T,A}/p_{T,T} \cos(\Delta\phi)$). The results

20 Jiangyong Jia

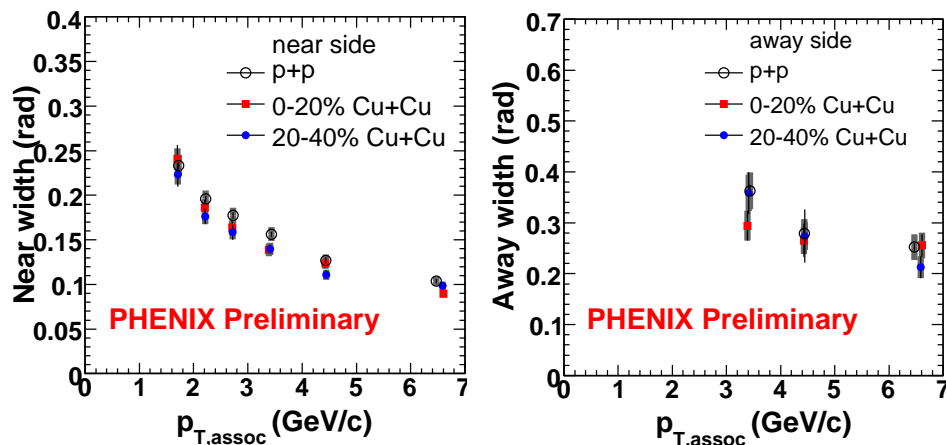


Fig. 18. The near side and away side jet gauss width for p+p, 0-20% and 20-40% Cu+Cu collisions.

from 0-20% central Cu+Cu collisions are shown in the left panel of Fig.19. I_{AA} at the near side is consistent with 1 in the full x_E range of 0.1-1.4; the away side I_{AA} starts at slightly above 1 at small x_E , and gradually decreases towards larger x_E , at $x_E > 0.4$ the suppression value approaches a constant of 0.5. This constant behavior is also seen by STAR in Au+Au collisions with N_{part} ¹. The level of suppression was found to be similar to single particle R_{AA} . Since the single particle R_{AA} in Au+Au and Cu+Cu collisions follows N_{part} scaling, we can ask whether I_{AA} also has similar scaling behavior. The right panel of Fig.19 shows the integrated I_{AA} in $0.4 < x_E < 1$ as function N_{part} , comparing with the integrated R_{AA} for the single particle. Assuming $\langle z \rangle \sim 0.7$ for leading π^0 s, the original jets should be around $5/0.7=7$ GeV/c. Thus the I_{AA} of the away side should be directly comparable to the single particle at $p_T > 7$ GeV/c. In reality, since the π^0 R_{AA} is flat at $p_T > 4$ GeV/c, the exact values of the jet energy for high p_T π^0 s are not important. Near side I_{AA} is around one in all centralities, consistent with surface emission picture. Away side I_{AA} shows a suppression that has a similar centrality dependence in N_{part} relative to single particle suppression. This is rather surprising given that the away side jet travels more medium than the single particles in the naive jet absorption picture. Probably suggesting that the simple geometrical bias argument in Section3.5 is too naive. In jet quenching picture, the suppression is due to the energy degradation of the high p_T jets. The suppression factor R_{AA} depends on both the energy loss itself as well as on the input parton spectra shape. For the single particle, the expected N_{binary} scaled p+p spectra have a typical power-law shape with a power of 8. In the di-hadron correlation, the away side spectra associated with the leading particles have much flatter distribution with a much smaller power. Thus for the same amount of energy loss for single jet and away side jet conditional to the near side jet, the suppression level observed for I_{AA} could be well less than

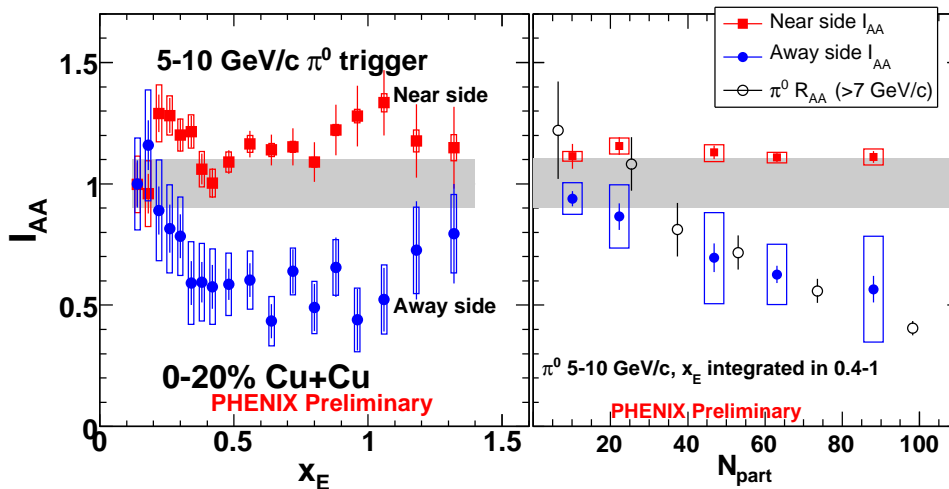


Fig. 19. a) The I_{AA} as function of x_E in p+p and Au+Au for near and away side; b) The I_{AA} for yield integrated in 0.4-1 as function of N_{part} , compared with suppression factor for high p_T π^0 .

the R_{AA} . If we follow the prescription in Ref. ³⁸, the fractional energy loss S_{loss} is related to R_{AA} as:

$$S_{loss} = 1 - R_{AA}(p_T)^{1/(n-1)} \quad \text{or} \quad R_{AA} = (1 - S_{loss})^{n-1} \quad (6)$$

The power “n” is 7.1 for single particle spectra in dN/dp_T . The power for the away side associated spectra can be determined from $p + p$ data ¹⁷ and it is about 4.8 in dN/dp_T . If the away side jet have same fraction energy loss as single particle, then we would expect:

$$S_{loss} = 1 - R_{AA}(p_T)^{1/(n_I-1)} = 1 - I_{AA}(p_T)^{1/(n_I-1)}. \quad (7)$$

$R_{AA} = 0.2$ in central Au+Au collisions would lead to $I_{AA} = R_{AA}^{(n_I-1)/(n_R-1)} = 0.37$, much bigger than R_{AA} . On the other hand, if we require $I_{AA} = R_{AA}$, then the away hadron energy loss fraction would be $S_{loss}^I = 1 - I_{AA}(p_T)^{1/(n_I-1)} = 0.345$, much bigger than the single hadron energy loss fraction $S_{loss}^R = 0.23$, as expected (about 50% more energy loss). If we apply the same trick to central Cu+Cu collisions, assuming $I_{AA} = R_{AA} = 0.5$, the fractional energy loss is would be $S_{loss}^R = 0.107$ and $S_{loss}^I = 0.167$ for single particle and away side jet, respectively.

4.2. γ -hadron correlation

In high p_T hadron - hadron or π^0 -hadron correlation, the total jet energy is not known. Trigger hadron from normal jet fragmentation carries on average about 60-70% ($\langle z \rangle$) of the total jet energy. This effect is known as the trigger bias, which have been studied in detail in p+p and d+Au collisions ^{39,17}. The energy loss of triggering jet in the medium leads to additional bias effects, and since the energy

loss is dependent on path length, the trigger bias effects would also coupled with the collision geometry. Thus complicates the extraction of the medium effects. Direct photon (γ_{dir})- hadron correlation does not suffer from such limitations. γ_{dir} serves as the gauge of the jet energy and jet direction, allowing the direct study of the medium modification of the away side jets. In reality, $\gamma_{\text{dir}} - h$ correlation has its own difficulties and limitations. In particular, once have to deal with large decay γ background, non-hard-scattering contributions such as the fragmentation and bremsstrahlung and thermal radiation and small rate.

PHENIX has observed a p_T dependent direct photon excess above the decay background in central Au+Au collisions. A statistical subtraction method combined with the knowledge on the direct γ excess³⁷ is used to obtain the $\gamma_{\text{dir}} - h$ signal. Fig.20 show the hadron yield associated with direct photons in $p+p$ collisions for two partner p_T ranges. Near side is consistent with zero, and away side shows some finite excess. The $p+p$ data are compared with the expected values from the PYTHIA6.1 calculation with $k_T=2.5$ GeV/ c . Within the large systematic uncertainties, the data qualitatively agrees with the PYTHIA value.

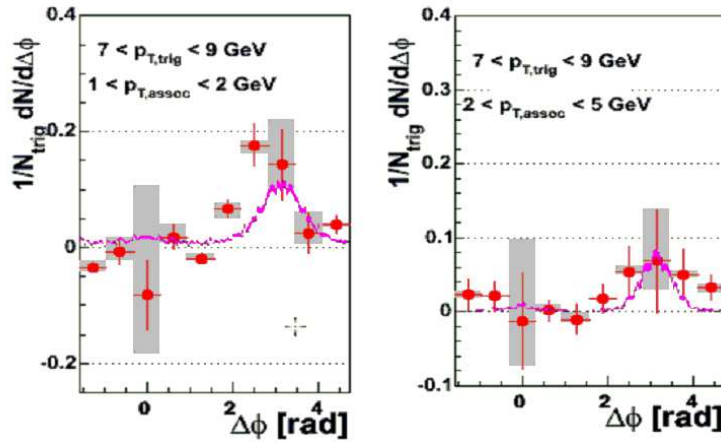


Fig. 20. The direct γ -h signal in $p+p$ collisions compared with PYTHIA simulation for 7-9 GeV/ c trigger γ and two partner p_T ranges.

Left panel of Fig.21⁴⁰ shows the comparison of the $\Delta\phi$ distribution of the PTY in $p+p$ and 0-20% central Au+Au collisions. The Au+Au data have smaller systematic errors, however the measurements are currently statistics limited, especially at around $\Delta\phi = \pi/2$ region. The Au+Au data seems to show a small positive yield at π , but the significance is only about 1σ level. One can reduce the statistic errors by integrating the away side yield in $\pi/2 < \Delta\phi < 3\pi/2$. The right panel of Fig.21 show the integrated yield for several trigger p_T regions with partner p_T fixed in 2-5 GeV/ c . $p+p$ data suggest a gradual increase of the PTY towards larger trigger p_T ,

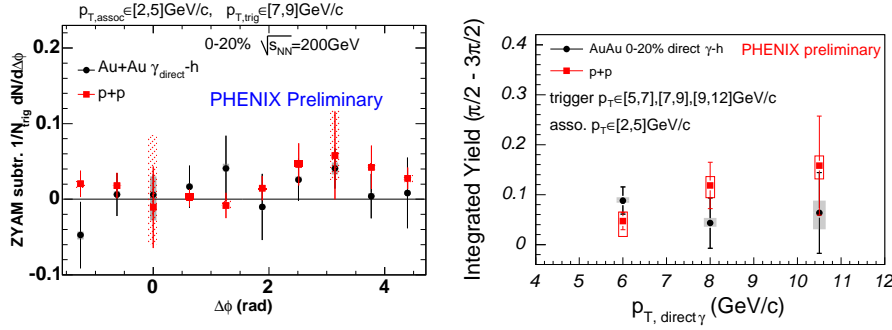


Fig. 21. a) The per-trigger yield for direct γ in central Au+Au (circles) and p+p (boxes). b) The integrated yield of the away side for several trigger direct γ ranges (data are plotted in the middle of the bin)

while the Au+Au data seems to stay relative flat and below the p+p level.

Overall, the results of the direct $\gamma - h$ correlation is still in a very qualitative stage, mainly due to limited statistics. However, the necessary methodologies have been developed and tested by PHENIX. It is only a question whether there will be sufficient statistics from future Au+Au runs. We might need the RHIC-II in order to do a really jet tomography measurement with direct photons.

5. Conclusion and outlook

PHENIX have mapped out the landscape of two particle azimuth correlation in heavy ion collisions as function of $p_{T,T}$, $p_{T,A}$, centrality, hadron species, \sqrt{s} and collision systems in different $\Delta\phi$ regions. The background subtracted “jet” pairs seems to come from four different components concentrated in different $\Delta\phi$ regions with their characteristic dependence on p_T , PID, \sqrt{s} etc. 1) A hard component around $\Delta\phi = 0$ that is consistent with jet fragmentation; 2) A soft and broad component around $\Delta\phi = 0$ that is consistent with the “Ridge” seen by STAR; 3) A hard component (“Head”) around $\Delta\phi = \pi$ consistent with fragmentation of away side jet; and 4) a soft component centered at $|\Delta\phi - \pi| \sim 1$ (“Shoulder”). The hard components are sensitive to the “quenching” of the (di-)jets by the medium. The hard component at the near side shows little modification, whereas the hard component at the away side are strongly suppressed, up to factor of 5 in central Au+Au collisions. The soft components (“Ridge” and “Shoulder”) represent the response of the medium to the jets, appearing as distortions of the shape and enhancements of the yield. These components are shown to be important at $p_T < 4$ GeV/c and have a particle composition that is closer to the bulk medium. The non-trivial evolutions of the near and away side shape/yield with p_T and \sqrt{s} are the results of the detailed interplay between the soft and hard components.

The four different components can have very different geometrical bias and

trigger bias. In a simple jet absorption picture where a very opaque medium is assumed, the near side hard component is emitted from the surface, $\langle L \rangle \sim 0$; the near side “Ridge” comes from jet close to the surface, $\langle L \rangle < R$ (R is the average radius of the medium); the away side “Shoulder” results from jet that traverses a large path length, $\langle L \rangle > R$; the path length for away side hard component can vary dramatically depends whether it is tangential emission or punch-through, $0 < \langle L \rangle < 2R$. One of the important future directions of the jet correlation is to quantitatively separate the four different components; and to study the detailed properties of each components. To fully understand the medium response, one need to address the question that whether the near side “Ridge” and away side “Shoulder” are of the same origin or not. A detailed mapping of the p_T , PID, charge and \sqrt{s} dependence would be very helpful in this regard. One can dial the path length by triggering on two high p_T triggers and correlate with the third soft hadrons, the “displaced” peak might be seen on both the near and away side⁴¹. However this is only possible if the high p_T have a significant punch-through component and the medium can not be very opaque. On the jet quenching part, high p_T correlation remains to be a good tomographic tool since it is less affected by the surface bias⁴. Both the centrality and reaction plane dependence of the jet correlation at high p_T would be very helpful in constraining the transport properties of the medium. In the meanwhile, we should continue to pursue the gamma-jet correlation with increased statistics and refined analysis techniques. Since it is less affected by the geometrical bias and trigger bias, even a statistics limited result could be very powerful in constraining various jet quenching models⁴².

References

1. J. Adams *et al.* [STAR Collaboration], arXiv:nucl-ex/0604018.
2. C. Loizides, arXiv:hep-ph/0608133.
3. T. Renk, arXiv:hep-ph/0602045.
4. H. Zhang, J. F. Owens, E. Wang and X. N. Wang, arXiv:nucl-th/0701045.
5. S. S. Adler *et al.* [PHENIX Collaboration], arXiv:nucl-ex/0507004.
6. A. Adare [PHENIX Collaboration], arXiv:nucl-ex/0611019.
7. J. Adams *et al.* [STAR Collaboration], Phys. Rev. Lett. **95**, 152301 (2005)
8. I. Vitev, Phys. Lett. B **630**, 78 (2005) [arXiv:hep-ph/0501255].
9. I. M. Dremin, JETP Lett. **30** (1979) 140 [Pisma Zh. Eksp. Teor. Fiz. **30** (1979) 152].
10. V. Koch, A. Majumder and X. N. Wang, arXiv:nucl-th/0507063.
11. J. Casalderrey-Solana, E. V. Shuryak and D. Teaney, arXiv:hep-ph/0411315.
12. N. Armesto, C. A. Salgado and U. A. Wiedemann, arXiv:hep-ph/0411341.
13. C. B. Chiu and R. C. Hwa, Phys. Rev. C **74**, 064909 (2006) [arXiv:nucl-th/0609038].
14. C. Adler *et al.* [STAR Collaboration], Phys. Rev. Lett. **90**, 082302 (2003)
15. C. A. Salgado and U. A. Wiedemann, Phys. Rev. Lett. **93**, 042301 (2004) [arXiv:hep-ph/0310079].
16. J. Jia, J. Phys. G **31**, S521 (2005)
17. S. S. Adler *et al.* [PHENIX Collaboration], Phys. Rev. C **73**, 054903 (2006) [arXiv:nucl-ex/0510021].
18. N. N. Ajitanand *et al.*, Phys. Rev. C **72**, 011902 (2005)

19. S. S. Adler *et al.* [PHENIX Collaboration], Phys. Rev. C **71**, 051902 (2005)
20. J. Jia [PHENIX Collaboration], AIP Conf. Proc. **828**, 219 (2006) [arXiv:nucl-ex/0510019].
21. N. Grau [PHENIX Collaboration], Nucl. Phys. A **774**, 565 (2006)
22. M. Ploskon, Nucl. Phys. A **783**, 527 (2007)
23. J. T. Mitchell, arXiv:nucl-ex/0701062.
24. J. G. Ulery [STAR Collaboration], Nucl. Phys. A **783**, 511 (2007)
25. N. N. Ajitanand [PHENIX Collaboration], arXiv:nucl-ex/0511029.
26. N. N. Ajitanand [PHENIX Collaboration], Nucl. Phys. A **783**, 519 (2007); C. Zhang, QM2006 proceedings.
27. A. Adare [PHENIX Collaboration], arXiv:nucl-ex/0611016.
28. J. Bielcikova, arXiv:nucl-ex/0701047; Leon Gaillard, these proceedings.
29. M. Miller and R. Snellings, arXiv:nucl-ex/0312008.
30. X. i. Zhu, M. Bleicher and H. Stoecker, Phys. Rev. C **72**, 064911 (2005) [arXiv:nucl-th/0509081].
31. S. Manly *et al.* [PHOBOS Collaboration], Nucl. Phys. A **774**, 523 (2006) [arXiv:nucl-ex/0510031].
32. R. S. Bhalerao and J. Y. Ollitrault, arXiv:nucl-th/0607009.
33. C. Loizides [the PHOBOS Collaboration], arXiv:nucl-ex/0701049;
34. P. Sorensen [STAR Collaboration], arXiv:nucl-ex/0612021.
35. S. S. Adler *et al.* [PHENIX Collaboration], Phys. Rev. Lett. **94**, 232302 (2005)
36. J. Jia [PHENIX Collaboration], Nucl. Phys. A **783**, 501 (2007).
37. S. S. Adler *et al.* [PHENIX Collaboration], Phys. Rev. Lett. **98**, 012002 (2007)
38. S. S. Adler [PHENIX Collaboration], arXiv:nucl-ex/0611007.
39. S. S. Adler *et al.* [PHENIX Collaboration], Phys. Rev. D **74**, 072002 (2006)
40. J. Jin, QM2006 proceedings.
41. T. Renk and K. J. Eskola, arXiv:hep-ph/0610059.
42. T. Renk, Phys. Rev. C **74**, 034906 (2006) [arXiv:hep-ph/0607166].